P12.175 Spatial Resolution of a Meteorological Radar Network Consisting of High Range and Temporal Resolution Radars

Eiichi Yoshikawa[1,2], Satoru Yoshida[1], Takeshi Morimoto[1], Tomoo Ushio[1], Zen Kawasaki[1,3], Tomoaki Mega[4], and V. Chandrasekar[2]
Osaka University[1], Colorado State University[2],
Egypt-Japan University of Science and Technology[3], Kyoto University[4]

1. INTRODUCTION

We have been proposing and developing a weather radar network consisting of the Ku-band BroadBand Radars (BBR), which is a short-range pulse-Doppler radar with remarkably high resolution (range and temporal resolution of several meters and 1 min per one volume scan, respectively) to detect and analyze small-scale weather phenomena such as localized scattered thunderstorms, tornadoes, and downbursts. Now we have two BBRs installed in Osaka area, Japan, and one more BBR is installing.

Compared with conventional long-range (100 through 450 km) weather radars at S-, C- or X-band, a short-range (up to tens of kilometers) weather radar network has significant advantages to observe those small-scale phenomena. Generally, a shorter-range weather radar has higher temporal resolution with more samples (since it needs shorter transit time), and with lower unobservable altitudes due to earth's curvature. Also in this observation strategy, radar nodes are installed with a baseline length which is comparable with a maximum observation range of radars. Therefore, there are large overlapped observation area in which several radar nodes simultaneously and multi-directionally observe precipitation from different sites and provide us additional information, for example, accurate reflectivity and 2- or 3-D wind field.

It is important to understand the characteristics of the Ku-BBR network for dealing with the obtained data. This presentation focuses simulation evaluations for the radar network property such as spatial distributions of the number of observable radar nodes, minimum cross-range resolution, sensitivity, and minimum observation altitude. In a weather radar network, these parameters are improved in a complementary manner between radar nodes [1]. And spatial resolution accomplished in preliminary data integration between radar nodes is presented. Multi-directional observation with high range resolution focuses the center point of a desired Cartesian grid and enhances spatial resolution.

Corresponding author address: Eiichi Yoshikawa, Osaka University, Division of Electrical, Electronic and Information Engineering, Osaka, Japan, 565-0871;
email: yoshikawa@comf5.comm.eng.osaka-u.ac.jp
Colorado State University, 1373 Campus Derivery, Fort Collins, CO, 80523-1373;
email: eyoshi@engr.colostate.edu

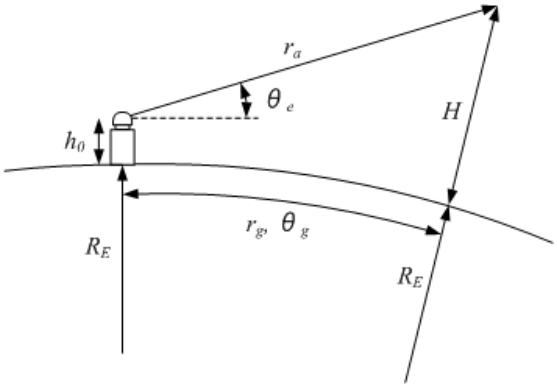

Figure 1. Radar observation on the spherical earth.

2. PROPERTIES OF THE KU-BBR NETWORK

2.1 RADAR NETWORK PARAMETERS IN THE SPHERICAL EARTH MODEL

Theory of weather radar networks is elaborated in [1]. In this presentation, properties of the Ku-BBR network, spatial distributions of the number of observable radar nodes, minimum cross-range resolution, sensitivity, and minimum observation altitude, are shown. These properties are briefly described below.

Figure 1 shows radar observation on the spherical earth. r_a, θ_e and h_0 are range from radar, elevation angle of antenna and installed altitude of radar, respectively. An altitude at a range of r_a which is affected by earth's curvature is H. r_g and θ_g, which are arc distance

Table I: Locational Characteristics of Radar Sites

Radar	Toyonaka	SEI	Nagisa
Latitude	34.804939°N	34.676993°N	34.840145°N
Longitude	135.455748°E	135.435054°E	135.659029°E
View	Fine	Poor (Many obstacles around notably south and north-east)	Fine
Remarks	-	Temporally installed	From Sep. 2011

and polar angle of the spherical earth, respectively, have a relation as

$$r_g = R_E \theta_g , \quad (1)$$

where R_E is the effective radius of the earth. Laws of sines and cosines express observation altitude as

$$H = \sqrt{(R_E + h_0)^2 + r_a^{\,2} + 2(R_E + h_0) r_a \sin\theta_e} - R_E , \quad (2)$$

where

$$r_a = (R_E + h_0) \frac{\sin\theta_g}{\cos(\theta_e + \theta_g)} . \quad (3)$$

The cross-range resolution b_s is defined as

$$b_s = r_a \theta_h , \quad (4)$$

where θ_h is -3-dB antenna beam width. And sensitivity $Z_{\min}$ is expressed as

$$Z_{\min} = 10\log\left(\frac{2}{c\tau} \frac{8\ln 2}{\pi\theta_h^{\,2}} \frac{\lambda^2 (4\pi)^3}{P_T G^2} \frac{P_{\min} r_a^{\,2}}{\pi^5 |k_w|^2} \right) , = 10\log\left(C_{\min} r_a^{\,2} \right) \quad (5)$$

where $P_{\min}$ is minimum detectable power, P_T is transmitting power, G is antenna gain, c is light speed, τ is transmitting pulse width, and λ is wave length. These parameters of the BBR system are totally determined as $C_{\min}$ by an experimental calibration through rain events with a use of a collocated disdrometer.

2.2 GENERAL PARAMETERS

The locational characteristics of the two BBRs (and another BBR which is installing now) are shown in Table I. One is installed on the top of a building in Toyonaka campus, Osaka University, Osaka, Japan (This radar is called "Toyonaka radar", hereafter). Another is installed on a building in Osaka works of Sumitomo Electric Industries, Ltd., Osaka, Japan (This is called "SEI radar", hereafter). The baseline interval of these radars is about 14.32 km. Table II shows two general observation modes of the BBR. The 15-km volume scanning mode has often been used in observation with one BBR. The 20-km volume scanning mode was designed for the two-BBR network observation, in which the larger observation range is accomplished instead of small deteriorations of temporal resolution and sensitivity.

Table II: General Observation Modes

Operation mode	15-km volume scanning	20-km volume scanning
Range resolution	7.5 m	
Temporal resolution (per volume scan)	64 s	70 s
Azimuth rotation speed	30.0 RPM	28.8 RPM
Elevation	0 – 90 deg	
Power	10 W	
Pulse length	160 μs	138 μs
Inter pulse priod	260 μs	271 μs
Pulses / segment	64	
Waveform	Linear up-chirp	
Band width	20 MHz (40 MHz in total)	
Weighting window	Raised-cosine window (α=0.1)	
Sensitivity in 10 km range	11.4 dBZ	12 dBZ

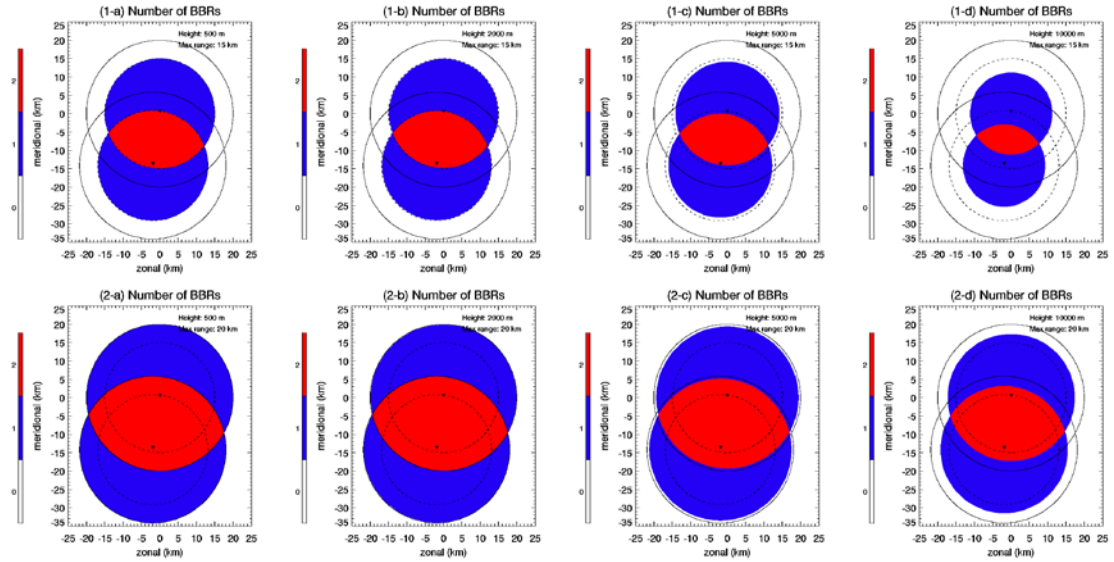

Figure 2. Spatial distributions of the number of observable radar nodes. In upper and lower panels (Panels (1- and (2-), maximum observation ranges are 15 and 20 km, respectively. Panels a), b), c) and d), from left to right, are on constant altitudes of 500, 2000, 5000, and 10000 m, respectively.

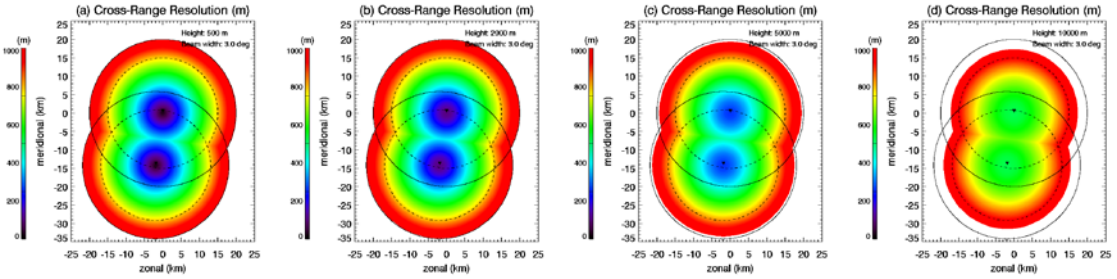

Figure 3. Spatial distributions of minimum cross-range resolution. Panels (a), (b), (c) and (d), from left to right, are on constant altitudes of 500, 2000, 5000, and 10000 m, respectively.

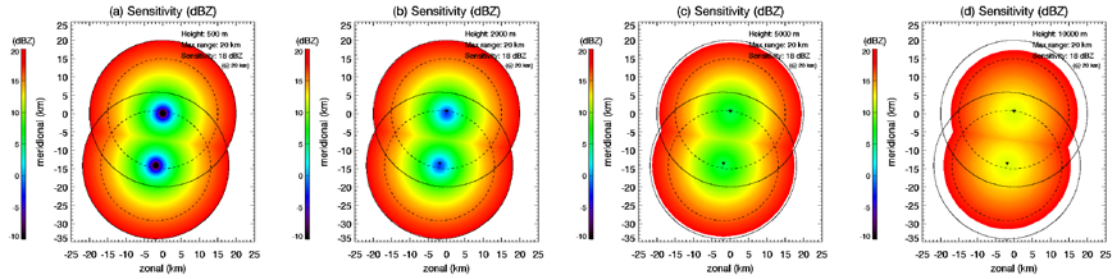

Figure 4. Spatial distributions of sensitivity. Panels (a), (b), (c) and (d), from left to right, are on constant altitudes of 500, 2000, 5000, and 10000 m, respectively.

2.3 PROPERTIES OF THE KU-BBR NETWORK

For simulation validations of the number of observable radar nodes, minimum cross-range resolution, sensitivity, and minimum observation altitude, it is assumed that each installed altitude of BBRs is 30 m and the earth's radius is 6370 km, and the 4/3 earth's radius model [2] is applied.

Figure 2 shows spatial distributions of the number of observable radar nodes with maximum observation ranges of 15 and 20 km (corresponding to Panels (1- and (2-, respectively) on constant altitudes of 500, 2000, 5000, and 10000 m (corresponding to Panels a), b), c) and d), respectively). Squares of overlapped area are 294 and 695 km^2 in the

15- and 20-km volume scanning mode, respectively in an altitude of 500 m. The 20-km mode has about 2.4 times larger overlapped area than the 15-km mode. Still in altitudes of 2000 and 5000 m, they have overlapped areas as large as in 500 m altitude. The volume scanning mode of 15 km, however, has small overlapped area whose square is 97 km^2 in 10000 m altitude. Thus, the two-BBR network with the 20-km mode is significantly appropriate to cover the lowest unobservable area of conventional long-range radars (below 2000 through 5000 m altitude).

Figure 3 shows spatial distribution of minimum cross-range resolution, in which Panels (a), (b), (c) and (d) are on constant altitudes of 500, 2000, 5000, and 10000 m, respectively. Cross-range resolution in almost all area are much larger than the range resolution of several meters. Although bigger size antennas are necessary to accomplish higher cross-range resolution, it is difficult for them to mechanically scan with a rapid rotation around 30 RPM, and also, sharper beams broaden spectral width of precipitation signals [2]. This result indicates that a contribution from radar network environment is still not sufficient to observe precipitation with 3-D high spatial resolution of several meters, and additional advanced signal processing is needed.

Figure 4 shows spatial distributions of sensitivity on constant altitudes of 500, 2000, 5000, and 10000 m (corresponding Panels (a), (b), (c) and (d), respectively). Spatial averages of sensitivity are 12.99, 13.23, 13.97, and 15.39 dBZ in an altitude of 500, 2000, 5000, and 10000 m, respectively, with the maximum (worst) sensitivity of 18 dBZ. In overlapped area, they are 9.36, 9.88, 11.42, and 14.03 dBZ. The two-BBR network has enough sensitivities for precipitation with a rainfall rate of 1 mm/h (roughly equals to 20 dBZ which is a design target of the Ku-BBR network) especially below 5000 m altitude as well as the number of observable radar nodes.

The affections of earth's curvature to the BBR network which is 24 m at most and 11 m on a spatial average within 20 km range. It is clear that the earth's curvature almost never affect to the two-BBR network.

3. SPATIAL RESOLUTION OF THE KU-BBR NETWORK

3.1 PRELIMINARY DATA INTEGRATION

Before integrating data obtained by BBRs at different sites, it is important to precisely correct precipitation attenuation. Or it is ideal that these two processes (precipitation attenuation correction and data integration) are performed at the same time. And advanced methods, which are or could be applied to radar network environments for these objectives, were already suggested [4], [5]. Developments of these kinds of signal processing methods for the Ku-BBR network are our future works and beyond the scope of this presentation. Here, preliminary data integration using geometric weighting to output initial observation results is presented. Precipitation attenuation is not considered to evaluate accomplished spatial resolution only.

At first, the obtained data on a polar coordinate whose origin is a radar is converted to a Cartesian coordinate with a use of a geometric weighting as below

$$Z_e^{(BBR_k)} = \sum_{n=1}^{4} w_c^{(k,n)} Z_e^{(k,n)} , \qquad (6)$$

where

$$w_c^{(k,n)} = \left[\frac{\hat{\theta}_{k,n}}{\theta_h - \hat{\theta}_{k,n}} \exp\left\{ 2\sqrt{2} \ln 2 \left(\frac{1}{2}\theta_h - \hat{\theta}_{k,n} \right) \right\} + 1 \right]^{-1} ,$$

$$\left[\frac{\hat{\phi}_{k,n}}{\phi_h - \hat{\phi}_{k,n}} \exp\left\{ 2\sqrt{2} \ln 2 \left(\frac{1}{2}\theta\phi_h - \hat{\phi}_{k,n} \right) \right\} + 1 \right]^{-1}$$

$$\hat{\theta}_{k,n} = \left| \theta_{k,n} - \theta \right| ,$$

$$\hat{\phi}_{k,n} = \left| \phi_{k,n} - \phi \right| . \qquad (7)$$

θ and ϕ are azimuth and elevation angle of the desired point from each radar. θ_h and ϕ_h are -3-dB beam width. *k* (= 1, 2) indicates each radar node in this case. The weighting function for data integration is expressed as

$$Z_e^{(INT)} = \frac{w_r^{(1)} Z_e^{(BBR_1)} + w_r^{(2)} Z_e^{(BBR_2)}}{w_r^{(1)} + w_r^{(2)}} , \qquad (8)$$

where

$$w_r^{(k)} = \left(\sum_{n=1}^{4} w_c^{(1)} g^{(k,n)}(\theta,\phi) \right)^{-1},$$

$$g^{(k,n)}(\theta,\phi) = \sum_{n=1}^{4} w_c^{(k,n)} \exp\left\{ -2\sqrt{2}\ln 2 \frac{\hat{\theta}_{k,n}^{\ 2} + \hat{\phi}_{k,n}^{\ 2}}{\theta_h^2} \right\}. \quad (9)$$

On the assumption that precipitation do not change in one volume scan due to the high temporal resolution of 1 min, an average of reflectivities obtained by several BBRs is also interpreted as an average of composite average functions [5]. Examples of a weighting average of composite average functions of BBR, which is normalized by a peak value, are shown in Figure 5 on base scan (in 2-D) for simplicity. These patterns are in a case that two BBRs with range resolution of 7.5 m (which is equivalent to transmitting a 20 MHz chirp signal) deployed in Cartesian coordinates of (7000, 0) and (-7000, 0) m. Panel (a) shows that the crossed pattern focuses precipitation at a desired point of (0, -5500) m, and the other undesired parts are suppressed. Panel (b), however, presents a case that two functions do not cross at a desired point of (2000, 0) m, in which resolution is never improved as in Panel (a). Three- or more-BBR network accomplish better patterns, and the suppression by weighting average in Z_e is several dBs at most. Although this is not enough in many cases of weather radar observation, realistic patterns of precipitation are shown in dealing with observed data as described in the next subsection.

3.2 AN EXAMPLE OF INTEGRATION FOR OBSERVED DATA

An example of data integration is shown in Figure 6. Panels (a) and (b) are observation results of Toyonaka and SEI radar on a constant altitude of 1000 m, in which precipitation attenuation is corrected by Hitchfeld-Bordan (HB) solution. Incorrectly retrieved reflectivities, which are often output by HB solution in a case with large path-integrated attenuation, are eliminated. Compared with this, integrated reflectivity in Panel (c) shows realistic pattern of precipitation due to the weighting average which focuses the center of each grid point as shown in Section 3.1. Meanwhile, Figure 7, a

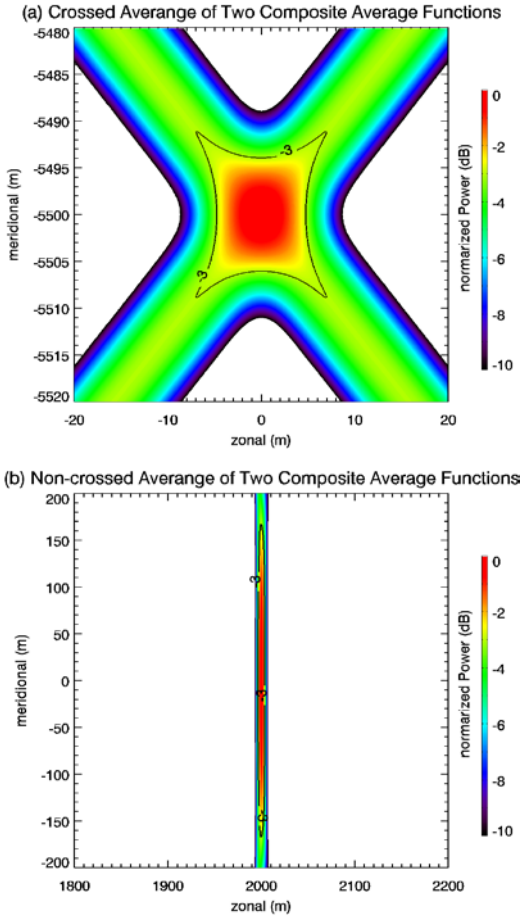

Figure 5. Composite average function of the BBR network. Panel (a) is a crossed pattern at a desired point of (0, -5500) m. Panel (b) is a non-crossed pattern at (2000, 0) m.

zoomed figure of Panel (c) in Figure 6, with zonal range from 1 to 6 km and meridional range from -10 to -5 km indicates many crossed patterns of averaged composite average function which are similar to the theoretical pattern in Panel (a) of Figure 5. This also means that the suppression by weighting average in Z_e is not sufficient in precipitation observation.

4. CONCLUSION

A simulation validation about radar network properties (spatial distributions of the number of observable radar nodes, minimum cross-range resolution, sensitivity, and minimum observation altitude) and accomplished spatial resolution by preliminary data integration in the two-BBR network installed in Osaka, Japan were presented. In the 20-km volume scanning mode the two-BBR

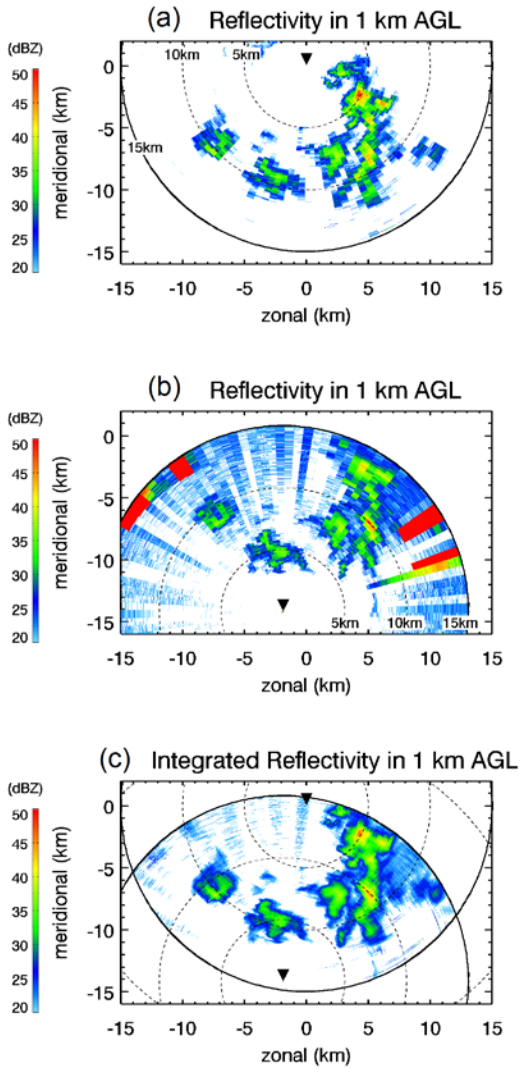

Figure 6. An example of observation results of Toyonaka and SEI radar and preliminary data integration result on a constant altitude of 1000 m.

network have an overlapped area whose square is 695 m^2 in 500 m altitude, and it is scarcely decreased until 5000 km. Likewise for sensitivity, its spatial averages in the whole observation area and the overlapped area are respectively below 14 dBZ and 11.5 dBZ with the maximum (worst) sensitivity of 18 dBZ. They are sufficient to observe 20 dBZ precipitation (roughly equals to a rainfall rate of 1 mm/h) which is a design target of the Ku-BBR network. The most unobservable altitude due to earth's curvature is 24 m at most. Thus, the Ku-BBR is appropriate to cover the lowest unobservable area of conventional long-range radars below 2000 through 5000 m altitude. A significant problem is the antenna

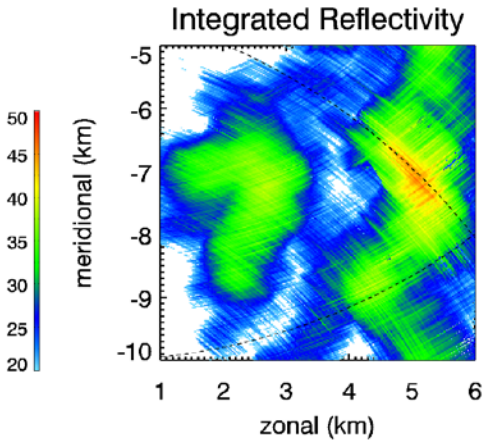

Figure 7. A zoomed figure of Panel (c) in Figure 6 with zonal range from 1 to 6 km and meridional range from -10 to -5 km.

beam width of 3 deg (equals to cross-range resolution of about 1000 m in a range of 20 km), which is much larger than the range resolution of several meters. Multi-directional and simultaneous observation between radar nodes and data integration with a use of simple geometric weighting average in Z_e improve resolution volume and show realistic structure of precipitation (though the results are preliminary and validations are needed). However, the enhancement of resolution volume is still not enough and the zoomed picture clearly shows the affection.

Advanced signal processings for precipitation attenuation correction and data integration could achieve better retrieval, and they are our near future works in addition to the validation for the integrated data indicated in this paper with collocated disdrometers.

ACKNOLEDGMENT

This work was supported by a grant from Ministry of Education, Science, and Sports and Culture, Japan, and Japan Society for the Promotion of Science (JSPS).

REFERENCES

[1] F. Junyent, and V. Chandrasekar, "Theory and characterization of weather radar networks," *J. Atmos. Ocean. Technol.*, vol. 26, pp. 474-491, 2009.

[2] R. J. Doviak, and D. S. Zrnic (1993), Doppler Radar and Weather Observations, Second edition, Dover Publications, Inc., New York, U.S.

[3] V. Chandrasekar and S. Lim, "Retrieval

reflectivity in a networked radar environment," *J. Atmos. Ocean. Technol.*, vol. 25, pp. 1755-1767, 2008.
[4] G. Zhang, Tian-You Yu, and R. J. Doviak, "Angular and range interferometry to refine weather radar resolution," *Radio Sciense*, vol. 40, 2005.
[5] V. N. Bringi, and V. Chandrasekar (2001), Polarimetric Doppler Weather Radar: Principles and Applications, pp. 211-293, Cambridge Univ. Press, Cambridge, U.K.